RESEARCH ARTICLE OPEN ACCESS

Non-Linear Dynamic Deformation of a Piezothermoelastic Laminate with Feedback Control System

Masayuki Ishihara*, Tetsuya Mizutani**, and Yoshihiro Ootao***
*(Graduate School of Engineering, Osaka Prefecture University, Japan)
**(Graduate School of Engineering, Osaka Prefecture University, Japan; Currently, Chugai Ro Co., Ltd.,Japan)
***(Graduate School of Engineering, Osaka Prefecture University, Japan)

ABSTRACT
We study the control of free vibration with large amplitude in a piezothermoelastic laminated beam subjected to a uniform temperature with a feedback control system. The analytical model is the symmetrically cross-ply laminated beam composed of the elastic and piezoelectric layers. On the basis of the von Kármán strain and the classical laminate theory, the governing equations for the dynamic behavior are derived. The dynamic behavior is detected by the electric current in the sensor layer through the direct piezoelectric effect. The electric voltage with the magnitude of the current multiplied by the gain is applied to the actuator layer to constitute a feedback control system. The governing equations are reduced by the Galerkin method to a Liénard equation with respect to the representative deflection, and the equation is found to be dependent on the gain and the configuration of the actuator. By introducing the Liénard's phase plane, the equation is analyzed geometrically, and the essential characteristics of the beam and stabilization of the dynamic deformation are demonstrated.
Keywords **-** feedback control, Liénard equation, piezothermoelastic laminate, vibration, von Kármán strain

I. INTRODUCTION

Piezoelectric materials have been extensively used as sensors and actuators to control structural configuration and to suppress undesired vibration owing to their superior coupling effect between elastic and electric fields. Fiber reinforced plastics (FRPs) such as graphite/epoxy are in demand for constructing lightweight structures because they are lighter than most metals and have high specific strength. Structures composed of laminated FRP and piezoelectric materials are often called piezothermoelastic laminates and have attracted considerable attention in fields such as aerospace engineering and micro electro-mechanical systems. For aerospace applications, structures must be comparatively large and lightweight. Because of this, they are vulnerable to disturbances such as environmental temperature changes and collisions with space debris. As a result, deformations due to these disturbances can be relatively large. Therefore, large deformations of piezothermoelastic laminates have been analyzed by several researchers [1-3].

The studies mentioned above [1-3] dealt with the static behavior of piezothermoelastic laminates. However, aerospace applications of these laminates involve dynamic deformation. Therefore, dynamic problems involving large deformations of piezothermoelastic laminates have become the focus of several studies [4-7]. In these studies [4-7], the dynamic behavior in the vicinity of the equilibrium state was analyzed. Dynamic deformation deviating arbitrarily from the equilibrium state is very important from a practical viewpoint for aerospace applications. Therefore, Ishihara et al. analyzed vibration deviating arbitrarily from the equilibrium state and obtained the relationship between the deflection of the laminate and its velocity under various loading conditions [8-10]. In these studies [8-10], methods to suppress undesired vibration due to known mechanical and thermal environmental causes were investigated; in other words, the manner of actuating, rather than the manner of sensing, was investigated.

In order to effectively suppress undesired vibration, it is important to consider both actuation and sensing and to integrate them into a feedback control system. Therefore, Ishihara et al. studied the control of the vibration of a piezothermoelastic laminate with a feedback control system under the framework of infinitesimal deformation [11-13]. However, as mentioned above, large deformation should be considered for applications of piezothermoelastic laminates.

In this study, therefore, we treat the control of the vibration with large amplitudes in a piezothermoelastic laminate with a feedback control system. The analytical model is a symmetric cross-ply laminated beam composed of fiber-reinforced laminae and two piezoelectric layers. The beam is simply supported at both edges, and it is exposed to a thermal environment. The undesired vibration of the laminate is transformed into electric current by the direct piezoelectric effect in one of the piezoelectric layers, which serves as a sensor. Then, in order to suppress the vibration, the electric voltage, with the

magnitude of the current multiplied by a gain, is applied to the other piezoelectric layer which is at the opposite side of the sensor and serves as an actuator. Large nonlinear deformation of the beam is analyzed on the basis of the von Kármán strain [14] and classical laminate theory. Equations of motion for the beam are derived using the Galerkin method [15]. Consequently, the dynamic deflection of the beam is found to be governed by a Liénard equation [16], which features a symmetric cubic restoring force and an unsymmetric quadratic damping force due to the geometric nonlinearity. The equation is geometrically studied in order to reveal the essential characteristics of the beam and to investigate how to stabilize the dynamic deformation.

II. THEORETICAL ANALYSIS

2.1 Problem

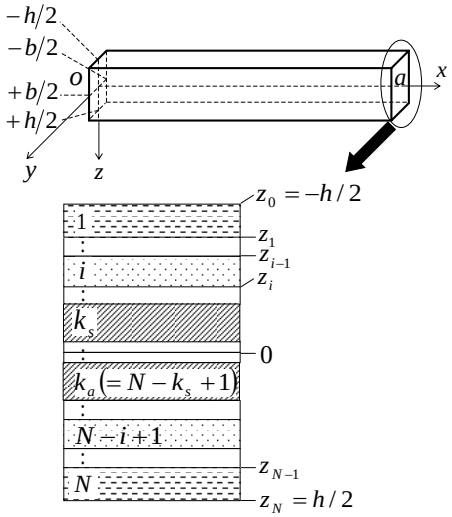

Fig. 1: analytical model

The model under consideration is a simply supported beam of dimensions $a \times b \times h$ and composed of N layers, as shown in Fig. 1. The k_s -th and k_a -th layers ($z_{k_s-1} \le z \le z_{k_s}$, $z_{k_a-1} \le z \le z_{k_a}$) exhibit piezoelectricity (with poling in the $+z$ or $-z$ direction), while the other layers do not. The beam is laminated in a symmetrical cross-ply manner.

The beam is subjected to temperature distributions $T_0(x,t)$ and $T_N(x,t)$ on the upper $(z=-h/2)$ and lower $(z=h/2)$ surfaces, respectively, as thermal disturbances that may vary with time t. Mechanical disturbance is modeled as the combination of the initial deflection and velocity.

To suppress the dynamic deformation due to the disturbances, the beam is subjected to the feedback control procedure: electric current $\dot{Q}_s(t)$ is detected in the k_s -th layer, which serves as a sensor to detect the deformation due to the disturbances; electrical potentials $\phi_{k_a-1}(x,t)$ and $\phi_{k_a}(x,t)$ determined on the basis of $\dot{Q}_s(t)$ are applied to the upper $(z=z_{k_a-1})$ and lower $(z=z_{k_a})$ surfaces, respectively, of the k_a -th layer, which serves as an actuator to suppress the deformation due to the disturbances. Moreover, in order to suppress the deformation effectively, the sensor and actuator are designed as a distributed sensor and actuator [17], i.e., the width of the electrodes for the k_s and k_a -th layers are variable as $b_s(x)=b\cdot f_s(x)$ and $b_a(x)=b\cdot f_a(x)$, respectively.

2.2 Governing Equations

In this subsection, the fundamental equations which govern the dynamic deformation of the beam are presented.

Based on the classical laminate theory, the displacements in the x and z directions are expressed, respectively, as

$$u = u^0(x,t) - z\frac{\partial w(x,t)}{\partial x}, \quad w = w(x,t), \tag{1}$$

where $u^0(x,t)$ and $w(x,t)$ denote the displacements on the central plane $(z=0)$. In order to treat nonlinear deformation, the von Kármán strain is introduced for the normal strain in the x direction as

$$\varepsilon_{xx} = \frac{\partial u}{\partial x} + \frac{1}{2}\left(\frac{\partial w}{\partial x}\right)^2 = \frac{\partial u^0}{\partial x} + \frac{1}{2}\left(\frac{\partial w}{\partial x}\right)^2 - z\frac{\partial^2 w}{\partial x^2}. \tag{2}$$

The electric field in the z direction is expressed by the electric potential $\phi(x,z,t)$ as

$$E_z = -\frac{\partial \phi}{\partial z}. \tag{3}$$

Assuming σ_{xx} , D_z , and T denote the normal stress in the x direction, the electric displacement in the z direction, and the temperature distribution, respectively, the constitutive equations for each layer are given as

$$\sigma_{xx} = E_i\varepsilon_{xx} - P_i(x)e_iE_z - \lambda_i T, \tag{4}$$

$$D_z = P_i(x)e_i\varepsilon_{xx} + \eta_i E_z + P_i(x)p_i T, \tag{5}$$

where E_i , η_i , e_i , λ_i , and p_i denote the elastic modulus, permittivity, piezoelectric constant, stress-temperature coefficient, and pyroelectric constant, respectively, in the i -th layer, and

$$\left.\begin{aligned} &e_{k_s} = e_{k_a}(<0),\ p_{k_s} = p_{k_a} \neq 0, \\ &e_i = 0,\ p_i = 0\ (i \neq k_a \text{ and } i \neq k_s) \end{aligned}\right\}. \tag{6}$$

The function $P_i(x)$ takes values of +1 and -1 in the portions with poling in the $+z$ and $-z$ directions, respectively.

By substituting (2) into (4) and integrating without and with multiplication with z, for $-h/2 \le z \le h/2$ we have the constitutive equations of the laminated beam as

$$\left.\begin{aligned} N_x &= A\left[\frac{\partial u^0}{\partial x}+\frac{1}{2}\left(\frac{\partial w}{\partial x}\right)^2\right]-N_x^T-N_x^E, \\ M_x &= -D\frac{\partial^2 w}{\partial x^2}-M_x^T-M_x^E \end{aligned}\right\}, \quad (7)$$

where N_x and M_x denote the resultant force and moment, respectively, defined by

$$\{N_x, M_x\}=\int_{-h/2}^{h/2}\sigma_{xx}\{1, z\}\mathrm{d}z. \quad (8)$$

N_x^T and M_x^T denote the thermally induced resultant force and moment, respectively, per unit width defined by

$$\left\{N_x^T, M_x^T\right\}=\sum_{i=1}^{N}\lambda_i\int_{z_{i-1}}^{z_i}T\{1, z\}\mathrm{d}z. \quad (9)$$

N_x^E and M_x^E denote the electrically induced resultant force and moment, respectively, per unit width. By considering $b_s(x)=b\cdot f_s(x)$ and $b_a(x)=b\cdot f_a(x)$, N_x^E and M_x^E are, respectively, defined by

$$\left.\begin{aligned} N_x^E &= P_{k_a}(x)e_{k_a}\int_{z_{k_a-1}}^{z_{k_a}}E_z\frac{b_a(x)}{b}\mathrm{d}z \\ &\quad + P_{k_s}(x)e_{k_s}\int_{z_{k_s-1}}^{z_{k_s}}E_z\frac{b_s(x)}{b}\mathrm{d}z \\ &= \left[P_{k_a}(x)f_a(x)\right]\cdot e_{k_a}\int_{z_{k_a-1}}^{z_{k_a}}E_z\mathrm{d}z \\ &\quad + \left[P_{k_s}(x)f_s(x)\right]\cdot e_{k_s}\int_{z_{k_s-1}}^{z_{k_s}}E_z\mathrm{d}z, \\ M_x^E &= P_{k_a}(x)e_{k_a}\int_{z_{k_a-1}}^{z_{k_a}}E_z z\frac{b_a(x)}{b}\mathrm{d}z \\ &\quad + P_{k_s}(x)e_{k_s}\int_{z_{k_s-1}}^{z_{k_s}}E_z z\frac{b_s(x)}{b}\mathrm{d}z \\ &= \left[P_{k_a}(x)f_a(x)\right]\cdot e_{k_a}\int_{z_{k_a-1}}^{z_{k_a}}E_z z\mathrm{d}z \\ &\quad + \left[P_{k_s}(x)f_s(x)\right]\cdot e_{k_s}\int_{z_{k_s-1}}^{z_{k_s}}E_z z\mathrm{d}z \end{aligned}\right\}. \quad (10)$$

From (10), it is found that $P_{k_a}(x)f_a(x)$ and $P_{k_a}(x)f_a(x)$, namely the profiles of poling directions and widths of the electrodes, determine the effective contribution of the electric field to the electrically induced resultant force and moment. A and D denote the extensional and bending rigidities, respectively, defined by

$$\{A, D\}=\sum_{i=1}^{N}\int_{z_{i-1}}^{z_i}E_i\{1, z^2\}\mathrm{d}z. \quad (11)$$

Equations of motion for the laminated beam are given as

$$\frac{\partial N_x}{\partial x}=0,\quad \frac{\partial^2 M_x}{\partial x^2}+N_x\frac{\partial^2 w}{\partial x^2}=\rho h\frac{\partial^2 w}{\partial t^2}, \quad (12)$$

where ρ is defined by

$$\rho=\frac{1}{h}\sum_{i=1}^{N}\rho_i\int_{z_{i-1}}^{z_i}\mathrm{d}z, \quad (13)$$

and denotes the mass density averaged along the thickness direction.

By substituting (7) into (12), we have the equations which govern displacements u^0 and w as

$$\left.\begin{aligned} &L_1(u^0, w)=\frac{\partial}{\partial x}\left(N_x^T+N_x^E\right), \\ &\rho h\frac{\partial^2 w}{\partial t^2}+L_2(u^0, w)= \\ &-\frac{\partial^2}{\partial x^2}\left(M_x^T+M_x^E\right)-\left(N_x^T+N_x^E\right)\frac{\partial^2 w}{\partial x^2} \end{aligned}\right\}, \quad (14)$$

where the definitions of differentiation operators L_1 and L_2 are given as

$$\left.\begin{aligned} L_1(u^0, w) &= A\left(\frac{\partial^2 u^0}{\partial x^2}+\frac{\partial w}{\partial x}\frac{\partial^2 w}{\partial x^2}\right), \\ L_2(u^0, w) &= -A\left[\frac{\partial u^0}{\partial x}+\frac{1}{2}\left(\frac{\partial w}{\partial x}\right)^2\right]\frac{\partial^2 w}{\partial x^2}+D\frac{\partial^4 w}{\partial x^4} \end{aligned}\right\}. \quad (15)$$

Because the beam is simply supported at both edges, the mechanical boundary conditions are expressed as

$$u^0=0,\ w=0,\ M_x=0;\ x=0, a. \quad (16)$$

The thermally induced resultant force and moment, N_x^T and M_x^T, and the electrically induced resultant force and moment, N_x^E and M_x^E, must be determined in order to solve (14). Assuming that the thickness of the beam h is sufficiently small compared to its length a, the temperature distribution is considered to be linear with respect to the thickness direction, and it is given as

$$\left.\begin{aligned} T(x, z, t) &= \frac{1}{2}\left[T_N(x, t)+T_0(x, t)\right] \\ &\quad + \frac{z}{h}\left[T_N(x, t)-T_0(x, t)\right] \end{aligned}\right\}. \quad (17)$$

Substituting (17) into (9) gives

$$\left.\begin{aligned} N_x^T &= h\frac{1}{2}\left[T_N(x, t)+T_0(x, t)\right]\sum_{i=1}^{N}\lambda_i\left(\frac{z_i}{h}-\frac{z_{i-1}}{h}\right), \\ M_x^T &= h^2\left[T_N(x, t)-T_0(x, t)\right]\sum_{i=1}^{N}\lambda_i\frac{1}{3}\left[\left(\frac{z_i}{h}\right)^3-\left(\frac{z_{i-1}}{h}\right)^3\right] \end{aligned}\right\}. \quad (18)$$

By assuming the thicknesses of the k_s-th and k_a-th layers are sufficiently small compared to its length a, the electric field distributions in both layers are considered to be linear with respect to the thickness direction, and they are given as

$$\left.\begin{aligned}
&\phi(x,z,t)=\phi_{k_s-1}(x,t)\\
&\quad+\left[\phi_{k_s}(x,t)-\phi_{k_s-1}(x,t)\right]\frac{z-z_{k_s-1}}{z_{k_s}-z_{k_s-1}}:\\
&\quad z_{k_s-1}\le z\le z_{k_s};\\
&\phi(x,z,t)=\phi_{k_a-1}(x,t)\\
&\quad+\left[\phi_{k_a}(x,t)-\phi_{k_a-1}(x,t)\right]\frac{z-z_{k_a-1}}{z_{k_a}-z_{k_a-1}}:\\
&\quad z_{k_a-1}\le z\le z_{k_a}
\end{aligned}\right\}. \qquad (19)$$

By substituting (3), (6), and (19) into (10), we have

$$\left.\begin{aligned}
N_x^E&=-\left[P_a(x)f_a(x)\right]\cdot e_{k_a}\left[\phi_{k_a}(x,t)-\phi_{k_a-1}(x,t)\right]\\
&\quad-\left[P_s(x)f_s(x)\right]\cdot e_{k_s}\left[\phi_{k_s}(x,t)-\phi_{k_s-1}(x,t)\right],\\
M_x^E&=-\left[P_a(x)f_a(x)\right]\\
&\quad\cdot e_{k_a}\left[\phi_{k_a}(x,t)-\phi_{k_a-1}(x,t)\right]\frac{z_{k_a}+z_{k_a-1}}{2}\\
&\quad-\left[P_s(x)f_s(x)\right]\\
&\quad\cdot e_{k_s}\left[\phi_{k_s}(x,t)-\phi_{k_s-1}(x,t)\right]\frac{z_{k_s}+z_{k_s-1}}{2}
\end{aligned}\right\}, \qquad (20)$$

where P_{k_a} and P_{k_s} are rewritten as P_a and P_s, respectively, for brevity.

In summary, (14) combined with (18) and (20) and the boundary conditions expressed by (16) are the equations that govern u^0 and w, that is, the dynamic deformation of the beam. Note that the applied electric potentials $\phi_{k_a-1}(x,t)$ and $\phi_{k_a}(x,t)$ are determined on the basis of the electric current $\dot{Q}_s(t)$. $\dot{Q}_s(t)$ reflects the dynamic deformation of the beam, and the manner in which $\dot{Q}_s(t)$ reflects this dynamic deformation is explained in the following subsection. The procedures to determine $\phi_{k_a-1}(x,t)$ and $\phi_{k_a}(x,t)$ are provided in Subsection 2.5.

2.3 Sensor Equation

The detected electric current $\dot{Q}_s(t)$ is related to the dynamic deformation of the beam through the direct piezoelectric effect of the sensor layer. By considering $b_s(x)=b\cdot f_s(x)$, the electric charge $Q_s(t)$ is evaluated by

$$\left.\begin{aligned}
Q_s(t)=\frac{1}{2}\Bigg[&\int_0^a (D_z)_{z=z_{k_s-1}}\, b\cdot f_s(x)\,dx\\
&+\int_0^a (D_z)_{z=z_{k_s}}\, b\cdot f_s(x)\,dx\Bigg]
\end{aligned}\right\}. \qquad (21)$$

By substituting (2), (3), (5), (17), and (19) into (21), differentiating the result with respect to t, and applying the *virtual short condition*

$$\phi_{k_s}(x,t)=\phi_{k_s-1}(x,t), \qquad (22)$$

we have

$$\left.\begin{aligned}
&\dot{Q}_s(t)\\
&=\int_0^a\Bigg\langle e_{k_s}\left[\frac{\partial \dot{u}^0}{\partial x}+\frac{\partial w}{\partial x}\frac{\partial \dot{w}}{\partial x}-\frac{z_{k_s}+z_{k_s-1}}{2}\frac{\partial^2 \dot{w}}{\partial x^2}\right]\\
&\quad+p_{k_s}\left\{\frac{1}{2}\left[\dot{T}_N(x,t)+\dot{T}_0(x,t)\right]\right.\\
&\quad\left.+\frac{z_{k_s}+z_{k_s-1}}{2h}\left[\dot{T}_N(x,t)-\dot{T}_0(x,t)\right]\right\}\Bigg\rangle bP_s(x)f_s(x)\,dx
\end{aligned}\right\}. \qquad (23)$$

It should be noted that $\dot{Q}_s(t)$ can be detected under the *virtual short condition* of (22) by a current amplifier [17], for example. Thus, the detected electric current $\dot{Q}_s(t)$ is related to the dynamic deformation of the beam.

2.4 Galerkin Method

The Galerkin method [15] is used to solve (14) under the condition described by (16) because (15) is a set of simultaneous *nonlinear* partial differential equations. Trigonometric functions are chosen as the trial functions to satisfy (16), and the considered displacements are expressed as the series

$$\left\{u^0,w\right\}=\sum_{m=1}^{\infty}\left\{u_m(t),w_m(t)\right\}\sin\alpha_m x, \qquad (24)$$

where

$$\alpha_m=\frac{m\pi}{a}. \qquad (25)$$

Then, the Galerkin method is applied to (14) to obtain

$$\left.\begin{aligned}
&\int_0^a\left[L_1\left(u^0,w\right)-\frac{\partial}{\partial x}\left(N_x^T+N_x^E\right)\right]\sin\alpha_{m'}x\,dx=0,\\
&\int_0^a\Bigg[\rho h\frac{\partial^2 w}{\partial t^2}+L_2\left(u^0,w\right)+\frac{\partial^2}{\partial x^2}\left(M_x^T+M_x^E\right)\\
&\quad+\left(N_x^T+N_x^E\right)\frac{\partial^2 w}{\partial x^2}\Bigg]\sin\alpha_{m'}x\,dx=0:\\
&m'=1,2,\ldots,\infty
\end{aligned}\right\}. \qquad (26)$$

Moreover, the distributions of temperature on both surfaces of the beam and those of the electric potential on both surfaces of the k_a-th layer are assumed to be uniform. Thus, one has

$$\left.\begin{aligned}
&T_0(x,t)\equiv T_0(t),\quad T_N(x,t)\equiv T_N(t),\\
&\phi_{k_a-1}(x,t)\equiv\phi_{k_a-1}(t),\quad \phi_{k_a}(x,t)\equiv\phi_{k_a}(t)
\end{aligned}\right\}. \qquad (27)$$

Substituting (22) and (27) into (18) and (20) gives

$$\left.\begin{aligned}
N_x^T&=h\frac{1}{2}\left[T_N(t)+T_0(t)\right]\sum_{i=1}^{N}\lambda_i\left(\frac{z_i}{h}-\frac{z_{i-1}}{h}\right),\\
M_x^T&=h^2\left[T_N(t)-T_0(t)\right]\sum_{i=1}^{N}\lambda_i\frac{1}{3}\left[\left(\frac{z_i}{h}\right)^3-\left(\frac{z_{i-1}}{h}\right)^3\right],\\
N_x^E&=N_{x,0}^E\left[P_a(x)f_a(x)\right],\\
M_x^E&=M_{x,0}^E\left[P_a(x)f_a(x)\right]
\end{aligned}\right\}, \qquad (28)$$

where

$$\left.\begin{aligned} N_{x,0}^{E} &= -e_{k_a}\left[\phi_{k_a}(t)-\phi_{k_a-1}(t)\right], \\ M_{x,0}^{E} &= -e_{k_a}\left[\phi_{k_a}(t)-\phi_{k_a-1}(t)\right]\frac{z_{k_a}+z_{k_a-1}}{2} \end{aligned}\right\}. \quad (29)$$

In order to satisfy (16), M_x^T and M_x^E are evaluated by using their Fourier series expansions as

$$\left\{M_x^T, M_x^E\right\} = \sum_{m=1}^{\infty}\left\{M_{x,m}^T(t), M_{x,m}^E(t)\right\}\sin\alpha_m x, \quad (30)$$

where $M_{x,m}^T(t)$ and $M_{x,m}^E(t)$ are given as

$$\left\{M_{x,m}^T(t), M_{x,m}^E(t)\right\} = \frac{2}{a}\int_0^a\left\{M_x^T, M_x^E\right\}\sin\alpha_m x\,\mathrm{d}x. \quad (31)$$

Moreover, in order to construct a modal actuator [17], the profiles of poling direction and the width of the electrode in the k_a-th layer are designed to be

$$\left[P_a(x)f_a(x)\right] = \sin\alpha_{m_a}x. \quad (32)$$

Then, from (28) and (32), one has

$$N_x^E = N_{x,0}^E\sin\alpha_{m_a}x, \quad M_x^E = M_{x,0}^E\sin\alpha_{m_a}x, \quad (33)$$

from which it is found that the actuator induces the m_a-th mode. By substituting (28) and (33) into (31), we have

$$\left.\begin{aligned} M_{x,m}^T(t) &= h^2\left[T_N(t)-T_0(t)\right] \\ &\cdot\sum_{i=1}^{N}\lambda_i\frac{1}{3}\left[\left(\frac{z_i}{h}\right)^3-\left(\frac{z_{i-1}}{h}\right)^3\right]\cdot\frac{4}{m\pi}\cdot\mathrm{mod}(m,2), \\ M_{x,m}^E(t) &= M_{x,0}^E\cdot\delta_{mm_a} \end{aligned}\right\}. \quad (34)$$

By substituting (15), (24), (25), (28), (30), and (33) into (26), the simultaneous nonlinear equations with respect to $u_m(t)$ and $w_m(t)$ are obtained as

$$\left.\begin{aligned} &A\left[\alpha_m^2 u_m + \sum_{m'=1}^{\infty}\sum_{i=1}^{\infty}\frac{1}{2}\alpha_{m'}^2\alpha_i w_{m'}w_i\delta_{m'im}\right] \\ &\quad + \frac{4}{\pi}\alpha_{m_a}N_{x,0}^E\delta'_{mm_a} = 0, \\ &\rho h\frac{\mathrm{d}^2 w_m}{\mathrm{d}t^2} + \alpha_m^2\left(D\alpha_m^2 - N_x^T\right)w_m \\ &\quad + \frac{4}{\pi}\sum_{m'=1}^{\infty}\alpha_{m'}^2 N_{x,0}^E w_{m'}\delta_{s,m_a m'm} \\ &\quad + \sum_{m'=1}^{\infty}\sum_{l=1}^{\infty}\frac{1}{2}A\alpha_{m'}^2\alpha_l\delta_{m'lm}w_{m'}u_l \\ &\quad + \sum_{m'=1}^{\infty}\sum_{i=1}^{\infty}\sum_{k=1}^{\infty}\frac{1}{8}A\alpha_{m'}^2\alpha_i\alpha_k\Delta_{c,ikm'm}w_{m'}w_i w_k \\ &\quad = \alpha_m^2\left(M_{x,m}^T + M_{x,0}^E\cdot\delta_{mm_a}\right): \\ &m = 1,2,\ldots,\infty \end{aligned}\right\}, \quad (35)$$

where the definitions of δ'_{ij}, δ_{ijk}, $\delta_{s,ijk}$, and $\Delta_{c,ijkl}$ are given in the previous paper [8]. Moreover, by eliminating $u_m(t)$ from (35), we obtain the simultaneous nonlinear ordinary differential equations with respect to $w_m(t)$ $(m = 1,2,3,\ldots,\infty)$ as

$$\left.\begin{aligned} &\rho h^2\frac{\mathrm{d}^2}{\mathrm{d}t^2}\left(\frac{w_m}{h}\right) + k_m^L\left(\frac{w_m}{h}\right) + \sum_{m'=1}^{\infty}k_{m,m'm_a}^A\left(\frac{w_{m'}}{h}\right) \\ &\quad + \sum_{m'=1}^{\infty}\sum_{i=1}^{\infty}\sum_{k=1}^{\infty}k_{m,m'ik}^N\left(\frac{w_{m'}}{h}\right)\left(\frac{w_i}{h}\right)\left(\frac{w_k}{h}\right) = p_m + p_m^A: \\ &m = 1,2,\ldots,\infty \end{aligned}\right\}, \quad (36)$$

where

$$\left.\begin{aligned} &k_m^L\left(=k_m^L(t)\right) = h\alpha_m^2\left(D\alpha_m^2 - N_x^T\right), \\ &k_{m,m'm_a}^A\left(=k_{m,m'm_a}^A(t)\right) \\ &\quad = h\alpha_{m'}^2\frac{4}{\pi}\left[\delta_{s,m_a m'm} - \sum_{l=1}^{\infty}\frac{\alpha_{m_a}\delta_{m'lm}\delta'_{lm_a}}{2\alpha_l}\right]N_{x,0}^E, \\ &k_{m,m'ik}^N = \frac{1}{8}h^3 A\alpha_{m'}^2\alpha_i\alpha_k\left(\Delta_{c,ikm'm} - \sum_{l=1}^{\infty}\frac{2\alpha_i}{\alpha_l}\delta_{ikl}\delta_{m'lm}\right), \\ &p_m\left(=p_m(t)\right) = \alpha_m^2 M_{x,m}^T, \\ &p_m^A\left(=p_m^A(t)\right) = \alpha_m^2 M_{x,0}^E\delta_{mm_a} \end{aligned}\right\}. \quad (37)$$

Moreover, in order to construct a modal sensor [17], the profiles of poling direction and the width of the electrode in the k_s-th layer are designed to be

$$\left[P_s(x)f_s(x)\right] = \sin\alpha_{m_s}x. \quad (38)$$

From (23), (24), and (27), we have

$$\left.\begin{aligned} \dot{Q}_s(t) &= e_{k_s}b\frac{2a}{\pi}\left[\sum_{m=1}^{\infty}\delta'_{m_s m}\alpha_m\dot{u}_m\right. \\ &\quad \left. - \sum_{m=1}^{\infty}\sum_{i=1}^{\infty}\delta_{c,imm_s}\alpha_i\alpha_m w_i\dot{w}_m + \frac{z_{k_s}+z_{k_s-1}}{2}\frac{\pi}{4}\alpha_{m_s}^2\dot{w}_{m_s}\right] \\ &\quad + p_{k_s}b\frac{2a}{\pi}\left\{\frac{1}{2}\left[\dot{T}_N(t)+\dot{T}_0(t)\right]\right. \\ &\quad \left. + \frac{z_{k_s}+z_{k_s-1}}{2h}\left[\dot{T}_N(t)-\dot{T}_0(t)\right]\right\}\frac{\mathrm{mod}(m_s,2)}{m_s} \end{aligned}\right\}. \quad (39)$$

Moreover, $u_m(t)$ in (39) is eliminated using (35) to give

$$\left.\begin{aligned} \dot{Q}_s(t) &= e_{k_s}b\frac{2a}{\pi}\left[-\frac{1}{A}\frac{4}{\pi}\sum_{l=1}^{\infty}\delta'_{m_s l}\delta'_{lm_a}\frac{\alpha_{m_a}}{\alpha_l}\dot{N}_{x,0}^E\right. \\ &\quad - \sum_{l=1}^{\infty}\sum_{i=1}^{\infty}\sum_{k=1}^{\infty}\delta'_{m_s l}\frac{\alpha_i\alpha_k}{2\alpha_l}\left(\alpha_i\delta_{ikl}+\alpha_k\delta_{kil}\right)w_i\dot{w}_k \\ &\quad \left. - \sum_{m=1}^{\infty}\sum_{i=1}^{\infty}\delta_{c,imm_s}\alpha_i\alpha_m w_i\dot{w}_m + \frac{z_{k_s}+z_{k_s-1}}{2}\frac{\pi}{4}\alpha_{m_s}^2\dot{w}_{m_s}\right] \\ &\quad + p_{k_s}b\frac{2a}{\pi}\left\{\frac{1}{2}\left[\dot{T}_N(t)+\dot{T}_0(t)\right]\right. \\ &\quad \left. + \frac{z_{k_s}+z_{k_s-1}}{2h}\left[\dot{T}_N(t)-\dot{T}_0(t)\right]\right\}\frac{\mathrm{mod}(m_s,2)}{m_s} \end{aligned}\right\}. \quad \ldots (40)$$

In order to extract the fundamental physical characteristics of the dynamic behavior of the beam, the most fundamental mode is treated as

$$u^0 = u_1(t)\sin\alpha_1 x, \quad w = w_1(t)\sin\alpha_1 x. \quad (41)$$

It should be noted that, from (25) and (41), $w_1(t)$ denotes the deflection of the beam at its center. In order to control the deformation described by (41), the electrode on the actuator is designed as

$$m_a = 1. \tag{42}$$

By considering (35) for $m=1$, one has

$$\left.\begin{aligned} & u_1 = 0, \\ & \rho h^2 \frac{\mathrm{d}^2}{\mathrm{d}t^2}\left(\frac{w_1}{h}\right) + \left(k_1^L + k_{1,1\,1}^A\right)\left(\frac{w_1}{h}\right) + k_{1,1\,1\,1}^N\left(\frac{w_1}{h}\right)^3 \\ & = p_1 + p_1^A \end{aligned}\right\}, \tag{43}$$

where k_1^L, $k_{1,1\,1}^A$, $k_{1,1\,1\,1}^N$, p_1, and p_1^A defined by (37) are reduced, using Eqs. (41) and (42), to

$$\left.\begin{aligned} & k_1^L\left(=k_1^L(t)\right) = h\alpha_1^2\left(D\alpha_1^2 - N_x^T\right), \\ & k_{1,1\,1}^A\left(=k_{1,1\,1}^A(t)\right) = -\frac{8}{3\pi}h\alpha_1^2 N_{x,0}^E, \\ & k_{1,1\,1\,1}^N = \frac{1}{8}h^3 A\alpha_1^4, \\ & p_1\left(=p_1(t)\right) = \alpha_1^2 M_{x,1}^T, \\ & p_1^A\left(=p_1^A(t)\right) = \alpha_1^2 M_{x,0}^E \end{aligned}\right\}. \tag{44}$$

Because the first mode is treated as in (41), the electrode on the sensor is so designed that

$$m_s = 1. \tag{45}$$

Then, from (39) and (41), one has

$$\left.\begin{aligned} \dot{Q}_s(t) = {} & e_{k_s} b\frac{2a}{\pi}\left[\frac{1}{3}\alpha_1^2 w_1\dot{w}_1 + \frac{z_{k_s}+z_{k_s-1}}{2}\frac{\pi}{4}\alpha_1^2\dot{w}_1\right] \\ & + p_{k_s} b\frac{2a}{\pi}\left\{\frac{1}{2}\left[\dot{T}_N(t)+\dot{T}_0(t)\right]\right. \\ & \left. + \frac{z_{k_s}+z_{k_s-1}}{2h}\left[\dot{T}_N(t)-\dot{T}_0(t)\right]\right\} \end{aligned}\right\}. \tag{46}$$

2.5 Equation for Feedback Control

In this subsection, we derive the equation to treat the control of the free vibration of the beam exposed to constant and uniform temperature.

We consider that the temperature on the upper and lower surfaces of the beam is constant and uniform as

$$T_N(t) = T_0(t) \equiv \Theta, \tag{47}$$

which leads to

$$T(x,z,t) = \Theta, \tag{48}$$

from (17), (27), and (47). From (28), (34), (46), and (47), we have

$$N_x^T = h\lambda_e\Theta, \quad M_x^T = 0, \quad M_{x,m}^T = 0, \tag{49}$$

$$\dot{Q}_s(t) = e_{k_s} b\frac{2a}{\pi}\left[\frac{1}{3}\alpha_1^2 w_1\dot{w}_1 + \frac{z_{k_s}+z_{k_s-1}}{2}\frac{\pi}{4}\alpha_1^2\dot{w}_1\right], \tag{50}$$

where

$$\lambda_e \equiv \sum_{i=1}^{N}\lambda_i\left(\frac{z_i}{h} - \frac{z_{i-1}}{h}\right) \tag{51}$$

represents the stress-temperature coefficient averaged with respect to the thickness direction.

We consider that the electric voltage applied to the actuator, $\left[\phi_{k_a}(t) - \phi_{k_a-1}(t)\right]$, is designed to be proportional to the electric current detected by the sensor, $\dot{Q}_s(t)$, as

$$\phi_{k_a}(t) - \phi_{k_a-1}(t) = -G\dot{Q}_s(t), \tag{52}$$

where G denotes the gain of the feedback control.

By substituting (29), (44), (49), and (52) into (43) and (50), we have

$$\left.\begin{aligned} & \rho h^2 \frac{\mathrm{d}^2}{\mathrm{d}t^2}\left(\frac{w_1}{h}\right) \\ & + \left[h\alpha_1^2\left(D\alpha_1^2 - h\lambda_e\Theta\right) + G\frac{8}{3\pi}h\alpha_1^2 e_p\dot{Q}_s(t)\right]\left(\frac{w_1}{h}\right) \\ & + \frac{h^3 A\alpha_1^4}{8}\left(\frac{w_1}{h}\right)^3 = -G\alpha_1^2 e_p\dot{Q}_s(t)z_p \end{aligned}\right\}, \tag{53}$$

$$\dot{Q}_s(t) = e_p b\frac{2a}{\pi}\left(\frac{\pi}{4}z_p - \frac{1}{3}w_1\right)\alpha_1^2\dot{w}_1, \tag{54}$$

where

$$e_p \equiv -e_{k_a} = -e_{k_s}(>0), \; z_p \equiv \frac{z_{k_a}+z_{k_a-1}}{2} = -\frac{z_{k_s}+z_{k_s-1}}{2} \tag{55}$$

... (55)

and z_p denotes the z coordinate of the central plane of the actuator. The case of $z_p > 0$ is treated for brevity. By introducing the nondimensional quantities as

$$\left.\begin{aligned} & W \equiv \frac{w_1}{h}, \; \zeta_p \equiv \frac{z_p}{h}, \; \tau \equiv \sqrt{\frac{hA\alpha_1^4}{8\rho}}t, \\ & \lambda \equiv \frac{8D}{h^2 A} - \frac{8}{hA\alpha_1^2}\lambda_e\Theta, \\ & I \equiv \sqrt{\frac{8\rho}{hA\alpha_1^4}}\frac{\dot{Q}_s(\tau)}{e_p h^2\alpha_1^2 ab}, \; \gamma \equiv \frac{8}{A}e_p^2 ab\sqrt{\frac{hA\alpha_1^4}{8\rho}}\cdot G \end{aligned}\right\}, \tag{56}$$

(53) and (54) are nondimensionalized, respectively, as

$$\frac{\mathrm{d}^2 W}{\mathrm{d}\tau^2} + \left(\lambda + \frac{8}{3\pi}\gamma I\right)W + W^3 = -\gamma I\zeta_p, \tag{57}$$

$$I = \frac{1}{2}\left(\zeta_p - \frac{4}{3\pi}W\right)\frac{\mathrm{d}W}{\mathrm{d}\tau}. \tag{58}$$

Thus, from (56)-(58), it is found that the nondimensional deflection W and the nondimensional electric current I are governed by nondimensional parameters λ, ζ_p $\left(0 < \zeta_p < 1/2\right)$, and γ, which denote the rigidity reduced by temperature, position of the actuator, and gain, respectively. By substituting (58) into (57), we have

$$\left.\begin{aligned} & \frac{\mathrm{d}^2 W}{\mathrm{d}\tau^2} + \gamma\frac{1}{2}\left(\zeta_p + \frac{8}{3\pi}W\right)\left(\zeta_p - \frac{4}{3\pi}W\right)\frac{\mathrm{d}W}{\mathrm{d}\tau} \\ & + \lambda W + W^3 = 0 \end{aligned}\right\}. \tag{59}$$

It is found that (59) has a set of equilibrium solutions

$$W = 0, \tag{60}$$

for $\lambda > 0$ and

$$W = 0, \pm\sqrt{|\lambda|}, \tag{61}$$

for $\lambda < 0$. Solutions described by (60) and (61) are different in nature. In this study, we consider that the temperature is lower than a critical value Θ_{cr} as

$$\Theta < \Theta_{cr}, \tag{62}$$

where Θ_{cr} is defined by

$$\Theta_{cr} = \frac{\alpha_1^2 D}{\lambda_e h}. \tag{63}$$

From (56), (62), and (63), it is found that the condition described by (62) leads to the condition

$$\lambda > 0, \tag{64}$$

which makes the linear rigidity in (59) positive. It should be noted that the temperature described by (63) is referred to as the buckling temperature.

In order to extract the governing parameters under (64), nondimensional quantities are introduced as

$$x \equiv \frac{W}{\sqrt{\lambda}},\ t \equiv \sqrt{\lambda}\tau,\ \mu \equiv \sqrt{\lambda}\gamma,\ z \equiv \frac{3\pi}{16}\frac{\zeta_p}{\sqrt{\lambda}}, \tag{65}$$

where x, t, μ, and z denote the nondimensional quantities of the deflection, time, gain, and actuator's position, respectively, and x, z, and t are different from the coordinates and the time variable defined in Subsection 2.1. Hereafter, x, z, and t are employed in the sense of (65) for brevity. Then, (59) is nondimensionalized as

$$\frac{\mathrm{d}^2 x}{\mathrm{d}t^2} + \mu f(x,z)\frac{\mathrm{d}x}{\mathrm{d}t} + g(x) = 0, \tag{66}$$

where functions $f(x,z)$ and $g(x)$ are defined as

$$f(x,z) \equiv -\frac{16}{9\pi^2}(x+2z)(x-4z),\ g(x) = x + x^3. \tag{67}$$

The equation with the form of (66) is known as Liénard's equation [16]. Particularly, if $g(x)$ is replaced with a linear function x and $f(x,z)$ with a symmetric function (x^2-1), (66) is referred to as van der Pol equation. The cubic term in $g(x)$ defined by (67) is derived from the nonlinear term $N_x \frac{\partial^2 w}{\partial x^2}$ in (12) combined with (7). The function $f(x,z)$ defined by (67) is unsymmetric with respect to $x = 0$ because the weight of the nonlinear term $N_x \frac{\partial^2 w}{\partial x^2}$ in the left-hand side of (12) is different from that of the nonlinear term $\frac{1}{2}\left(\frac{\partial w}{\partial x}\right)^2$ in the second and third terms on the right-hand side of (2). In the context of this research, the first, second, and third terms on the left-hand side of (66) are the terms of inertia, damping, and restoring force of the system, respectively.

From (66) and (67), it is found that (66) has its sole equilibrium solution $x = 0$. We call the function $f(x,z)$ as the damping characteristic function in the sense that it describes the dependency of the damping intensity for a deflection x. A numerical example of the damping characteristic function $f(x,z)$ is shown in Fig. 2.

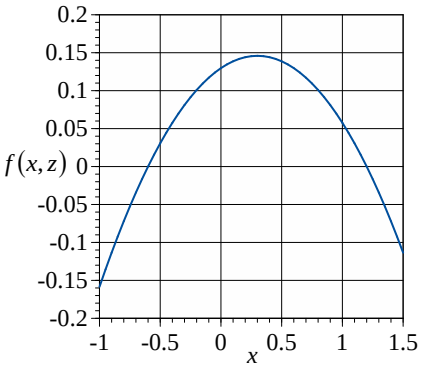

Fig. 2: damping characteristic function

Because $f(x,z)$ is positive in the vicinity of $x = 0$, it is found that the equilibrium solution $x = 0$ is locally stable for $\mu > 0$. Moreover, from (67) or Fig. 2, it is found that

$$f(x,z) > 0 \text{ for } -2z < x < 4z. \tag{68}$$

Therefore, the equilibrium solution $x = 0$ is expected to be not only locally but also globally stable within a certain range around $x = 0$. Conversely, from (67) or Fig. 2, it is found that

$$f(x,z) < 0 \text{ for } x < -2z \text{ or } x > 4z, \tag{69}$$

which gives the system negative damping for $\mu > 0$. In that case, it is expected that a vibration with relatively large amplitude will be unstable.

Therefore, it is important to determine the range of deformation in which the system is operated stably. For this purpose, the governing equation, (67), is analyzed geometrically by introducing the Liénard's phase plane [18] (x, y) that is governed by

$$\dot{x} = \mu[y - F(x,z)],\ \dot{y} = -\frac{1}{\mu}g(x), \tag{70}$$

where the overdot denotes differentiation with respect to t, and $F(x,z)$ is defined by

$$\left.\begin{aligned} F(x,z) &\equiv \int_0^x f(x,z)\mathrm{d}x \\ &= -\frac{16}{27\pi^2}x\left(x + \frac{\sqrt{105}-3}{2}z\right)\left(x - \frac{\sqrt{105}+3}{2}z\right) \end{aligned}\right\}. \tag{71}$$

It should be noted that elimination of y in (70) leads to the original governing equation, (67). From the first part of (70), we have

$$y = \frac{\dot{x}}{\mu} + F(x,z). \qquad (72)$$

Thus, we call y the *modified velocity* in the sense that it is related to the *actual velocity* $\dot{x}$. Figure 3 shows the characteristics of the phase plane governed by (70). The solid lines in red denote

$$x = 0,\ y = F(x,z), \qquad (73)$$

which make the right-hand sides of (70) null and are, therefore, called *nullclines*. From (70), it is found that the nullclines in (73) divide the phase plane shown in Fig. 3 into four parts by the signs of $\dot{x}$ and $\dot{y}$. The broken arrows in Fig. 3 denote the directions of the trajectories governed by (70). The examples of the trajectories are indicated by blue lines in Fig. 4. The point (x_0, y_0) denotes the initial combination of (x, y).

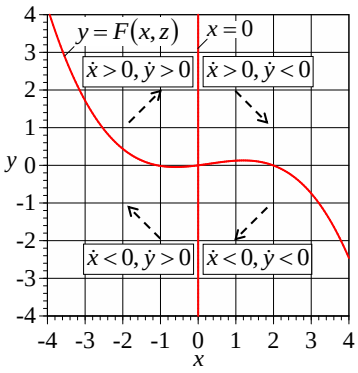

Fig. 3: characteristics of Liénard's phase plane

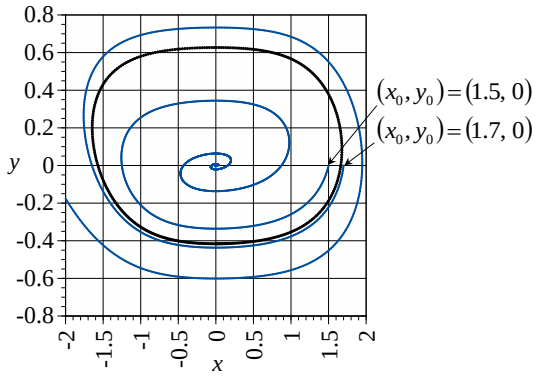

Fig. 4: examples of trajectories

From Fig. 4, it is found that a trajectory may move toward or away from the equilibrium point $(x, y) = (0,0)$; in other words, the vibration may be stable or unstable. Therefore, it is expected that there is a closed boundary line that divides the stability as indicated by the broken line in Fig. 4. Such a line is usually called the *limit cycle*. It should be noted that the limit cycle is numerically obtained by changing the variables as $t \to -t$ in (70) for an arbitrary initial condition and, therefore, is dependent on parameters μ and z.

III. Numerical Results

As stated in Subsection 2.5, the limit cycle divides the stability in the phase plane. In other words, the trajectories that start inside the cycle lead to the sole equilibrium point $(x, y) = (0,0)$. Therefore, it is important to investigate the shape of the limit cycle. In this section, the effects of parameters μ and z on the shape of the phase plane are investigated.

3.1 Effect of Gain

In this subsection, the effect of the nondimensional parameter μ, which represents the gain of the feedback control, is described.

Figures 5 (a)-(d) show the limit cycles for various values of μ, in which the blue solid lines and red broken lines denote the limit cycles and the nullclines determined by (73), respectively. In Fig. 5, the limit cycles are found to be horizontal $(\mathrm{d}y/\mathrm{d}x = \dot{y}/\dot{x} = 0)$ or vertical $(\mathrm{d}x/\mathrm{d}y = \dot{x}/\dot{y} = 0)$ on the nullclines, which is found also from (70) and (73). Moreover, as shown in Fig. 3, the abscissa or the ordinate of a limit cycle becomes maximum or minimum on the nullclines.

From Fig. 5, it is found that, as the value of μ increases, the shape of the limit cycle converges to the shape shown in Fig. 5 (d). This tendency for $\mu >> 1$ is explained using (70) as follows. At a point such as $[y - F(x,z)] \sim \mathrm{O}(1)$, equation (70) implies $|\dot{x}| \sim \mathrm{O}(\mu) >> 1$ and $|\dot{y}| \sim \mathrm{O}(\mu^{-1}) << 1$, which corresponds to the quasi-horizontal branches of the cycle. In these branches, the trajectory quickly and quasi-horizontally moves to the nullcline $y = F(x,z)$ because $|\dot{x}| \sim \mathrm{O}(\mu) >> 1$ and $|\dot{y}| \sim \mathrm{O}(\mu^{-1}) << 1$. However, once the trajectory approaches the nullcline so closely that $[y - F(x,z)] \sim \mathrm{O}(\mu^{-2})$, then $\dot{x}$ and $\dot{y}$ become comparable as $\dot{x} \sim \mathrm{O}(\mu^{-1})$ and $\dot{y} \sim \mathrm{O}(\mu^{-1})$, and the trajectory moves nearly along the nullcline.

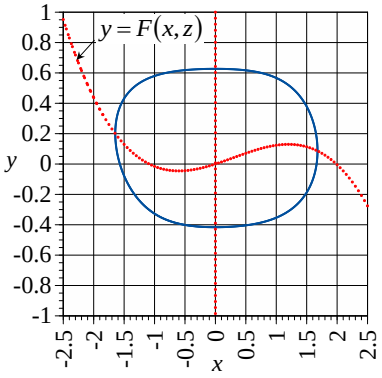

(a) $\mu = 5$

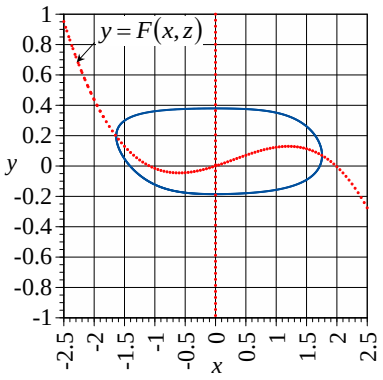

(b) $\mu = 10$

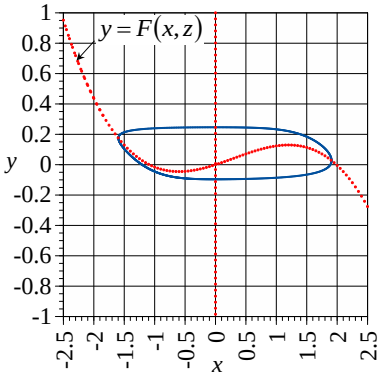

(c) $\mu = 20$

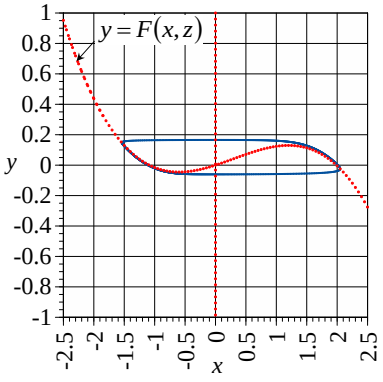

(d) $\mu = 50$

Fig. 5: effect of gain on limit cycle $(z = 0.3)$

As $|x|$ increases, $|\dot{y}|$ increases compared with $|\dot{x}|$. Therefore, the trajectory approaches the nullcline and finally crosses the nullcline vertically, as shown in Fig. 3.

The maximum and minimum values of the abscissa and ordinate of a limit cycle are important characteristics of the cycle because they correspond to the limit within which the system is operated safely. To be more precise, the maximum and minimum values of the abscissa correspond to the upper and lower limits of the initial position when the initial *modified velocity* is zero, and those of the ordinate correspond to the upper and lower limits of the initial *modified velocity* when the initial position is zero. In view of these facts, we refer to the maximum and minimum values of the abscissa of a limit cycle as the upper and lower limits of the initial position, respectively, and refer to those of the ordinate of the cycle as the upper and lower limits of the initial *modified velocity*, respectively. In addition, we refer to the maximum and minimum values of the *actual velocity* $\dot{x}$ along the limit cycle as the upper and lower limits of the *actual velocity*, respectively.

Figure 6 shows the variations of the upper and lower limits of the position, *modified velocity*, and *actual velocity* with parameter μ, in which subscripts "upper" and "lower" correspond to the upper and lower limits, respectively. From Figs. 6 (a) and (b), it is found that, as μ increases, the upper and lower limits of the position and *modified velocity* change monotonically and converge to certain values as explained previously. From Fig. 6 (c), it is found that the upper limit of the *actual velocity* increases as μ increases and that the lower limit has a local maximum.

Usually, a larger value of μ is preferable in order to quickly pull the system back to the equilibrium point $(x, y) = (0,0)$. However, as shown in x_{lower} in Fig. 6 (a), the limit within which the system is operated safely may decrease. In this regard, the safe ranges of the initial position x_{initial}, *modified velocity* y_{initial}, and *actual velocity* $\dot{x}_{\text{initial}}$ are investigated. From Fig. 6, it is found that the system is stable for an arbitrary value of μ when x_{initial}, y_{initial}, and $\dot{x}_{\text{initial}}$ satisfies

$$x_{\text{lower}}(\mu >> 1) < x_{\text{initial}} < x_{\text{upper}}(\mu = 0), \quad (74)$$

$$y_{\text{lower}}(\mu >> 1) < y_{\text{initial}} < y_{\text{upper}}(\mu >> 1), \quad (75)$$

and

$$\dot{x}_{\text{lower}}(\mu \cong 13) < \dot{x}_{\text{initial}} < \dot{x}_{\text{upper}}(\mu = 0), \quad (76)$$

respectively.

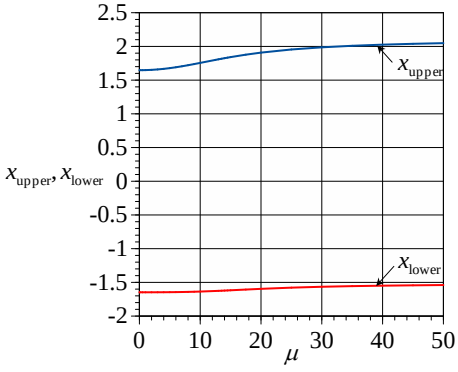

(a) position

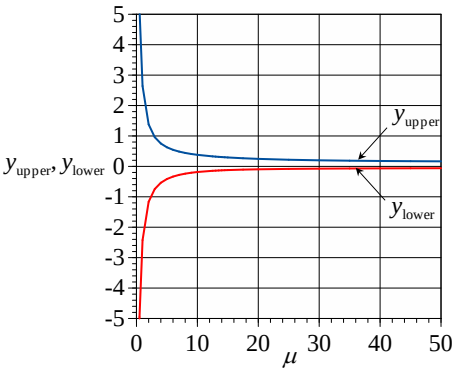

(b) modified velocity

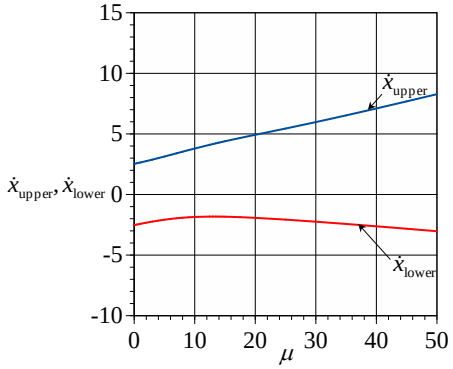

(c) actual velocity

Fig. 6: variations of upper and lower limits with gain $(z = 0.3)$

3.2 Effect of Actuator Position

In this subsection, the effect of the nondimensional parameter z, which represents the actuator position in the laminated beam, is described.

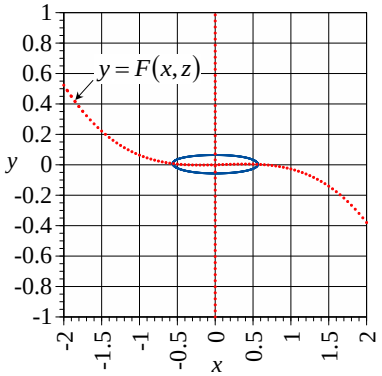

(a) $z = 0.1$

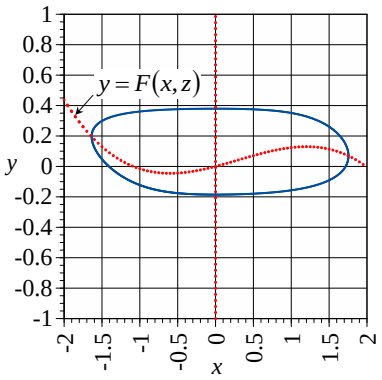

(b) $z = 0.3$

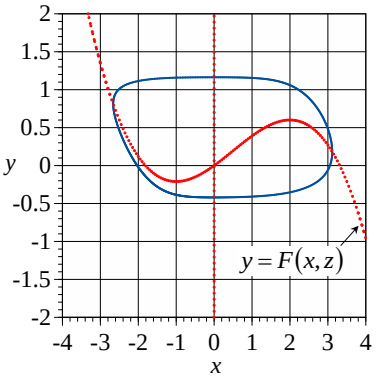

(c) $z = 0.5$

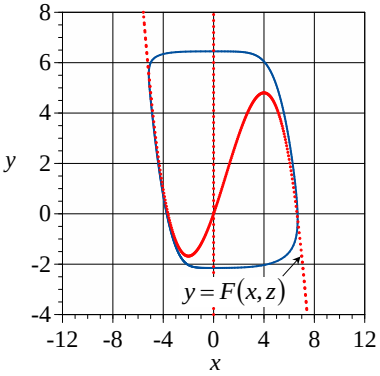

(d) $z = 1$

Fig. 7: effect of actuator position on limit cycle $(\mu = 10)$

Figures 7 (a)-(d) show the limit cycles for various values of z, in which the blue solid lines and red broken lines denote the limit cycles and the nullclines determined by (73), respectively. Figures 8 (a), (b), and (c) shows the variation of the upper and lower limits of the position, *modified velocity*, and *actual velocity*, respectively, with parameter z.

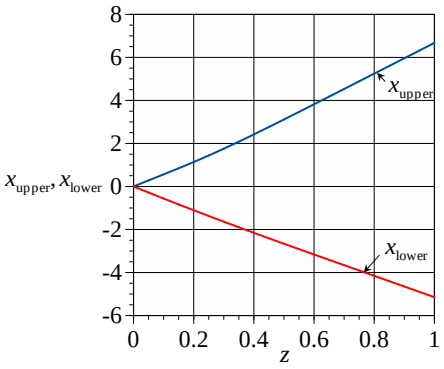

(a) position

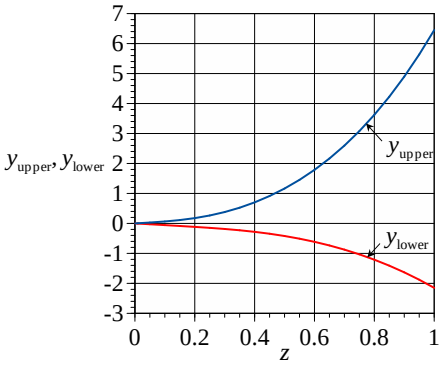

(b) modified velocity

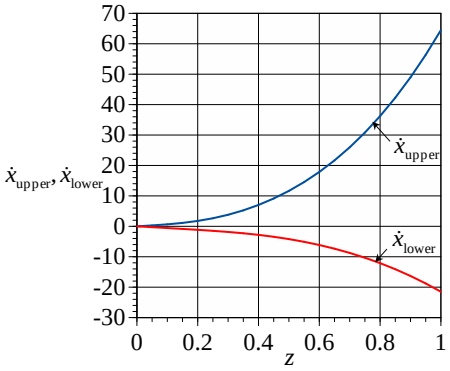

(c) actual velocity

Fig. 8: variations of upper and lower limits with actuator position $(z = 0.3)$

From Figs. 7 and 8, it is found that the range in which the system is operated safely becomes wider as z increases. This is explained as follows. From (55), (56), and (65), parameter z corresponds to the actuator position in the laminated beam. From (28) and (29), it is found that, the farther out the actuator is installed, the greater the electrically induced resultant moment becomes.

IV. CONCLUSION

In this study, we treated the control of the free vibration with large amplitude in a piezothermoelastic laminated beam subjected to a uniform temperature with a feedback control system. On the basis of the von Kármán strain, classical laminate theory, and the Galerkin method, the beam was found to be governed by a Liénard equation dependent on the gain of the feedback control and the configuration of the actuator. By introducing the Liénard's phase plane, the equation was analyzed geometrically, and the essential characteristics of the beam and stabilization of the dynamic deformation were clearly demonstrated.

The above-mentioned simplification of the Liénard equation is significantly advantageous because the essential dependence of the system behavior on the system parameters is clearly demonstrated. Moreover, the above-mentioned approach is effective for nonlinear problems because their explicit solutions are rather difficult to obtain. However, our approach is not suitable for cases in which coupling among plural modes is involved.

The findings in this study are considered to serve as fundamental guidelines in the design of piezothermoelastic laminate used for lightweight structures vulnerable to large deformation due to mechanical and thermal disturbances.

REFERENCES

[1] A. Mukherjee and A. S. Chaudhuri, Piezolaminated beams with large deformations, *International Journal of Solids and Structures, 39(17),* 2002, 4567-4582.

[2] H. S. Shen, Postbuckling of shear deformable laminated plates with piezoelectric actuators under complex loading conditions, *International Journal of Solids and Structures, 38(44-45),* 2001, 7703-7721.

[3] H. S. Shen, Postbuckling of laminated cylindrical shells with piezoelectric actuators under combined external pressure and heating, *International Journal of Solids and Structures, 39(16),* 2002, 4271-4289.

[4] H. S. Tzou and Y. Zhou, Dynamics and control of nonlinear circular plates with piezoelectric actuators, *Journal of Sound and Vibration, 188(2),* 1995, 189-207.

[5] H. S. Tzou and Y. H. Zhou, Nonlinear piezothermoelasticity and multi-field actuations, part 2, control of nonlinear deflection, buckling and dynamics, *Journal of Vibration and Acoustics, 119,* 1997, 382-389.

[6] M. Ishihara and N. Noda, Non-linear dynamic behavior of a piezothermoelastic laminated plate with anisotropic material properties, *Acta Mechanica 166(1-4),* 2003, 103-118.

[7] M. Ishihara and N. Noda, Non-linear dynamic behavior of a piezothermoelastic laminate considering the effect of transverse shear, *Journal of Thermal Stresses, 26(11-12),* 2003, 1093-1112.

[8] M. Ishihara and N. Noda, Non-linear dynamic behaviour of a piezothermoelastic

laminate, *Philosophical Magazine 85(33-35),* 2005, 4159-4179.

[9] Y. Watanabe, M. Ishihara, and N. Noda, Nonlinear transient behavior of a piezothermoelastic laminated beam subjected to mechanical, thermal and electrical load, *Journal of Solid Mechanics and Materials Engineering, 3(5),* 2009, 758-769.

[10] M. Ishihara, Y. Watanabe, and N. Noda, Non-linear dynamic deformation of a piezothermoelastic laminate, in H. Irschik, M. Krommer, K. Watanabe, and T. Furukawa (Ed.), *Mechanics and model-based control of smart materials and structures* (Wien: Springer-Verlag, 2010) 85-94.

[11] M. Ishihara, N. Noda, and H. Morishita, Control of dynamic deformation of a piezoelastic beam subjected to mechanical disturbance by using a closed-loop control system, *Journal of Solid Mechanics and Materials Engineering 1(7),* 2007, 864-874.

[12] M. Ishihara, H. Morishita, and N. Noda, Control of dynamic deformation of a piezothermoelastic beam with a closed-loop control system subjected to thermal disturbance, *Journal of Thermal Stresses, 30(9),* 2007, 875-888.

[13] M. Ishihara, H. Morishita, and N. Noda, Control of the transient deformation of a piezoelastic beam with a closed-loop control system subjected to mechanical disturbance considering the effect of damping, *Smart Materials and Structures, 16(5),* 2007, 1880-1887.

[14] C. Y. Chia, *Nonlinear analysis of plates* (New York: McGraw-Hill, 1980).

[15] C. A. J. Fletcher, *Computational Galerkin method* (New York: Springer, 1984).

[16] S. H. Strogatz, *Nonlinear dynamics and chaos* (Boulder: Westview Press, 2001).

[17] C. -K. Lee, Piezoelectric laminates: Theory and experiments for distributed sensors and actuators, in H. S. Tzou and G. L. Anderson (Ed.), *Intelligent Structural Systems* (Dordrecht: Kluwer Academic Publishers, 1992) 75-168.

[18] N. Minorsky, *Nonlinear Oscillations* (Princeton: Van Nostrand, 1962).